Research Square

Preprints are preliminary reports that have not undergone peer review.
They should not be considered conclusive, used to inform clinical practice,
or referenced by the media as validated information.

COF-5-based TiO_2 and AuNP composites for UV/H_2O_2-assisted photocatalytic degradation of 4-nitrophenol

Keziah Janice Imanuela
Department of Chemical Engineering, Widya Mandala Surabaya Catholic University
Ronald Sanjaya
Department of Chemical Engineering, Widya Mandala Surabaya Catholic University
Alfin Kurniawan
Research Group for Advanced Materials & Sustainable Catalysis (AMSC), State Key Laboratory of Green Chemical Synthesis and Conversion, College of Chemical Engineering, Zhejiang University of Technology
Jindrayani Putro
jindrayani@ukwms.ac.id
Chemical Engineering Master Program, Faculty of Engineering, Widya Mandala Surabaya Catholic University https://orcid.org/0000-0002-1970-9314
Suryadi Ismadji
Department of Chemical Engineering, Widya Mandala Surabaya Catholic University
Astrid Rahmawati
Department of Applied Chemistry, Osaka Institute of Technology
Osamu Shimomura
Department of Applied Chemistry, Osaka Institute of Technology

Research Article

Keywords: COF-5, nitroaromatic, photodegradation, TiO2, Gold nanoparticle

Posted Date: September 1st, 2026

DOI: https://doi.org/10.21203/rs.3.rs-10396653/v1

License: This work is licensed under a Creative Commons Attribution 4.0 International License.
Read Full License

Abstract

Covalent organic frameworks (COFs) are porous crystalline materials with promising potential for photocatalytic environmental remediation. In this study, COF-5 and COF-5-based composites containing TiO_2 or Au nanoparticles were synthesized and evaluated for the photodegradation of 4-nitrophenol (4-NP) under UV/H_2O_2 irradiation. The formation of COF-5, TiO_2@COF-5, and AuNP@COF-5 was confirmed by XRD, SEM, HR-TEM, SAED, EDX, and XPS analyses. XRD patterns verified the characteristic low-angle reflections of COF-5 and the coexistence of anatase TiO_2 or face-centered cubic Au phases in the composites. HR-TEM, SAED, and EDX further confirmed the incorporation of TiO_2 and AuNPs into the COF-5 matrix, while XPS verified the presence of Ti 2p and Au 4f signals in the corresponding composites. Photocatalytic experiments were conducted using 4-NP as a model nitroaromatic pollutant under UV irradiation at 254 nm in the presence of H_2O_2. The photocatalytic activity followed the order TiO_2@COF-5 > AuNP@COF-5 > TiO_2 > AuNP > COF-5. Kinetic analysis showed that the biphasic first-order model provided the best fitting for all photocatalysts, with R^2 values of approximately 0.98–0.99, indicating a rapid initial degradation stage followed by a slower stage. The enhanced activity of TiO_2@COF-5 was attributed to the combined role of UV-active TiO_2 and the porous COF-5 framework, which improved substrate accessibility, interfacial interaction, and charge-transfer efficiency. These findings demonstrate the potential of COF-5-based composites for the degradation of nitroaromatic pollutants.

1. Introduction

Nitroaromatic compounds are widely used as intermediates in the manufacture of pharmaceuticals, dyes, pesticides, explosives, and other industrial chemicals. However, their toxicity, mutagenicity, carcinogenicity, and persistence have raised serious environmental and health concerns. Several nitroaromatic compounds have therefore been listed as priority pollutants by the United States Environmental Protection Agency (EPA) (Tiwari et al. 2019; Khan et al. 2023). Among them, 4-nitrophenol (4-NP) is particularly important because of its extensive use in the production of pesticides, analgesics, dyes, and pharmaceutical intermediates (Khan et al. 2023). The uncontrolled release of 4-NP into the environment can contaminate water and soil. It may cause adverse health effects, including respiratory problems, nausea, fatigue, and long-term damage to the nervous system, liver, and kidneys (Bilal et al. 2021). Therefore, the development of efficient and sustainable strategies for the removal or transformation of 4-NP is urgently needed to support environmental protection, public health, and safer chemical management.

In Indonesia, the issue of 4-NP contamination is closely linked to broader challenges in water pollution control, particularly from industrial wastewater, agricultural runoff, pesticide use, and insufficient treatment of organic pollutants. Although specific monitoring data for 4-NP in Indonesian water bodies remain limited, several studies have highlighted that pesticide-related pollutants and other hazardous organic compounds are relevant concerns in Indonesian river basins. For example, pesticide risk prioritization in the Upper Citarum River Basin showed that measured concentration data are often

unavailable in low- and middle-income countries such as Indonesia, underscoring the importance of risk-based screening for identifying priority pollutants (Utami et al. 2020). In addition, river pollution remains a significant environmental problem in Indonesia, while rivers remain important sources of water for domestic and other activities (Basuki et al. 2024). These conditions indicate that advanced treatment technologies for persistent organic contaminants, including nitrophenolic compounds such as 4-NP, are highly relevant to Indonesia's environmental remediation needs.

Heterogeneous photocatalysis has emerged as a promising strategy for the treatment of nitroaromatic pollutants, enabling light-driven chemical transformations under relatively mild conditions. In particular, the photocatalytic reduction of 4-NP into 4-aminophenol (4-AP) is attractive because 4-AP is a valuable intermediate for pharmaceutical and dye industries. This approach offers both environmental and economic benefits by reducing the toxicity of pollutants while converting hazardous compounds into value-added chemicals (Gu et al. 2023; Yadav et al. 2023). Therefore, the development of efficient photocatalytic materials is essential to improve light utilization, charge separation, substrate adsorption, and overall conversion efficiency. In this context, photocatalytic conversion is also consistent with the principles of sustainable chemistry, cleaner production, and circular resource utilization.

Covalent organic frameworks (COFs) have recently attracted considerable attention as crystalline porous materials with high surface area, tunable pore structures, and designable chemical functionalities. These characteristics make COFs promising candidates for photocatalysis and environmental remediation (Yadav et al. 2023). Among various COFs, COF-5 is one of the earliest boronate ester-linked COFs reported by Yaghi and co-workers (Côté et al. 2005). Its ordered porous structure may facilitate pollutant adsorption, substrate accessibility, and mass transfer during photocatalytic reactions. However, the use of COF-5 for the photocatalytic conversion of nitroaromatic pollutants, particularly 4-NP, remains underexplored.

In recent studies, COF-5 has attracted attention as a support material for titanium and gold to improve photodegradation performance. The formation of composites such as COF-5@TiO_2 and COF-5@AuNP can enhance catalytic activity through synergistic interactions between the porous COF structure and the active nanoparticles. In the COF-5@TiO_2 composite, TiO_2 particles dispersed on the COF-5 framework form a heterojunction that promotes efficient separation of photogenerated electron–hole pairs and increases photodegradation efficiency compared to pure TiO_2 (Zhou et al. 2023). Meanwhile, in the COF-5@AuNP composite, gold nanoparticles act as electron traps, facilitating charge transfer and suppressing recombination, thereby improving catalytic performance (Bi 2022). Therefore, the incorporation of TiO_2 or Au into the COF-5 framework is expected to provide higher photodegradation efficiency for nitroaromatic compounds compared to the use of single photocatalysts.

In this study, COF-5, TiO_2, AuNP, and COF-5-based composite photocatalysts are investigated for the photocatalytic reduction of 4-NP into 4-AP. The photocatalytic activities of the prepared materials are compared to elucidate the contribution of each component toward 4-NP conversion. By placing the study within the context of organic pollutant treatment and wastewater challenges in Indonesia, this

work is expected to contribute to sustainable environmental remediation, safer chemical production, pollution control, and the development of advanced photocatalytic materials for cleaner industrial applications.

2. Materials and methods

2.1. Materials

2,3,6,7,10,11-Hexahydroxytriphenylene, $C_{18}H_{12}O_6$ (95% purity) was purchased from Thermo Fisher Scientific (Germany), Benzene-1,4-diboronic acid, $C_6H_8B_2O_4$ (≥ 95% purity) was purchased from Sigma-Aldrich, (China), Methanol, CH_3OH (≥ 99,9% purity) was purchased from Supelco (Germany), 1,4-Dioxane, $C_4H_8O_2$ (≥ 99% purity) was purchased from Sigma-Aldrich (United States of America), Mesitylene, C_9H_{12} (97% purity) was purchased from Sigma-Aldrich (United States of America), Acetone, CH_3COCH_3 (≥ 99,9% purity) was purchased from Supelco (Germany), Titanium dioxide, TiO_2, (anatase phase) was purchased from Flew Solutions (Australia), Gold(III) chloride trihydrate, $HAuCl_4 \cdot 3H_2O$, (≥ 49% purity) was purchased from Sigma-Aldrich (United States of America), Trisodium citrate dihydrate, $HOC(COONa)(CH_2COONa)_2 \cdot 2H_2O$ (≥ 99% purity) was purchased from Supelco (Germany), Ethanol, C_2H_6O (≥ 99,9% purity) was purchased from Supelco (Germany), 4-Nitrophenol, $C_6H_5NO_3$ (≥ 99% purity) was purchased from Sigma-Aldrich (United States of America), 4-Aminophenol, C_6H_7NO (≥ 98% purity) was purchased from Sigma-Aldrich (United States of America) and Hydrogen peroxide, H_2O_2 (50% wt), was purchased from Merck (Germany).

2.2. Synthesis of COF-5

COF-5 was synthesized using a modified method based on previous studies (Ritchie et al. 2010; Smith et al. 2014). Briefly, 112 mg of 2,3,6,7,10,11-hexahydroxytriphenylene (HHTP, 0.345 mmol), 86 mg of benzene-1,4-diboronic acid (BDBA, 0.52 mmol), and 0.21 mL of methanol (5.2 mmol) were added to a mixed solvent of 1,4-dioxane and mesitylene at a volume ratio of 1:4 (v/v), with a total solvent volume of 43 mL, at room temperature [31]. The mixture was then sonicated for 10 min at room temperature to obtain a homogeneous dispersion. Subsequently, the reaction mixture was transferred into a Teflon-lined autoclave reactor and heated at 100°C for 48 h [30]. After completion of the reaction, the autoclave was allowed to cool naturally to room temperature. The resulting COF-5 product was then separated by centrifugation to obtain the precipitate. The precipitate was washed with acetone by centrifugation at 10,000 rpm for 10 min. This washing step was performed to remove residual reactants and unreacted solvents. Finally, the precipitate was dried in a vacuum oven at 60°C and 0.1 bar to obtain dry COF-5 powder.

2.3. Synthesis of Gold Nanoparticles (AuNP)

AuNPs were synthesized using the citrate-reduction method with trisodium citrate dihydrate as the reducing agent (Turkevich et al. 1951). Briefly, 20 mL of $HAuCl_4 \cdot 3H_2O$ solution (10^{-3} M) was heated to

80°C for 15 min under vigorous, continuous stirring. Subsequently, 2 mL of trisodium citrate dihydrate solution (1% w/v) was added to the precursor solution. The reaction mixture was heated to 80°C for 30 min until the solution turned wine-purple, indicating the formation of an AuNP suspension.

2.4. Synthesis of TiO_2@COF-5 and AuNP@ COF-5

TiO_2@COF-5 composites were synthesized using a modified method based on a previous study (Zhou et al. 2023). Briefly, 47.94 mg of anatase TiO_2 (0.6 mmol) was added to the COF-5 monomer solution. The resulting mixture was sonicated for 10 min at room temperature to obtain a homogeneous dispersion. Subsequently, the reaction mixture was transferred into a Teflon-lined autoclave reactor and heated at 100°C for 48 h. After the reaction was completed, the autoclave was allowed to cool naturally to room temperature. The resulting TiO_2@COF-5 suspension was then centrifuged to collect the precipitate. The obtained precipitate was washed with acetone by centrifugation at 10,000 rpm for 10 min to remove residual reactants and unbound species. Finally, the precipitate was dried in a vacuum oven at 60°C and 0.1 bar to obtain the dried TiO_2@COF-5 composite.

Similarly, the AuNP@COF-5 composite was prepared via an in situ incorporation approach using a pre-synthesized AuNP suspension. Briefly, 1 mL of the AuNP suspension was added to the COF-5 monomer solution, followed by ultrasonication for 10 min at room temperature to ensure uniform dispersion of the AuNPs within the reaction medium. The resulting mixture was then subjected to solvothermal treatment in a Teflon-lined autoclave at 100°C for 48 h. After the reaction, the autoclave was allowed to cool naturally to room temperature. The formed AuNP@COF-5 solid was collected by centrifugation and washed with acetone at 10,000 rpm for 10 min to remove residual monomers, solvents, and loosely attached AuNPs. Finally, the purified precipitate was dried in a vacuum oven at 60°C under 0.1 bar to obtain the AuNP@ COF-5 composite powder.

2.5. Photodegradation of 4-Nitrophenol

Photodegradation experiments were conducted using a reaction solution containing 50 mL of 4-nitrophenol (4-NP: 1,043 mg/L) and 2.84 mL of H_2O_2 solution (50 wt%). Subsequently, 10 mg of photocatalyst was added to the solution. An aliquot of the reaction mixture was then transferred into a cuvette for irradiation. The photodegradation process was performed in a UV irradiation chamber equipped with dual 254-nm UV lamps for 60 min. The absorbance of the solution was monitored at room temperature (25°C) using a UV–Vis spectrophotometer (UV-1700, Shimadzu, Japan). Measurements were recorded at 1 min intervals for the first 10 min, then at 5 min intervals until 60 min.

2.6. Characterizations

In this study, all synthesized materials were characterized using several analytical techniques. UV–Vis spectrophotometry was employed to record full-wavelength absorbance spectra and monitor absorbance changes at selected wavelengths during the 4-NP photodegradation process. X-ray diffraction (XRD) was used to evaluate the crystallinity and phase structure of the materials over a 2θ range of 3–80°. The XRD patterns of COF-5, TiO_2, AuNP, TiO_2@COF-5, and AuNP@COF-5 were analyzed

to confirm the successful formation of the corresponding materials and composites. The surface morphology of the samples was examined using scanning electron microscopy (SEM; Zeiss EVO, Germany) at an accelerating voltage of 20 kV and magnifications corresponding to a 1–2 μm scale range. The SEM images were further analyzed using ImageJ software to estimate the particle size of the materials. In addition, high-resolution transmission electron microscopy (HR-TEM) was performed to further investigate the composite structures, particularly the dispersion and interfacial characteristics of TiO_2 and AuNPs within or on the COF-5 framework. The HR-TEM analysis was also used to observe nanoscale morphological features and lattice fringes associated with the incorporated crystalline phases. X-ray photoelectron spectroscopy (XPS) was further conducted to analyze the surface chemical composition and electronic states of the composites, with particular emphasis on the binding energies of Ti and Au in TiO_2@COF-5 and AuNP@COF-5, respectively.

3. Results and discussions

3.1. Characterizations

The XRD pattern of COF-5 in Fig. 1(a) exhibits characteristic diffraction peaks at 2θ = 3.05°, 6.01°, 6.96°, and 9.59°, which are assigned to the (100), (200), (210), and (310) planes, respectively. These low-angle reflections confirm the formation of an ordered boronate ester-linked COF-5 framework, which is consistent with the typical diffraction features reported for crystalline COF-5 and other two-dimensional COFs (Côté et al. 2005). The crystallinity index of COF-5 was calculated to be 67.84%, indicating the formation of a relatively ordered framework structure.

The XRD pattern of anatase TiO_2 in Fig. 1(b) agrees well with the standard diffraction pattern of tetragonal anatase TiO_2. The prominent peaks observed at 2θ = 25.35° and 48.08° are assigned to the (101) and (200) planes, respectively, confirming the anatase phase of TiO_2 (Yaacob et al. 2019). The crystallinity index of TiO_2 was 45.11%, indicating moderate crystallinity. Meanwhile, the AuNPs in Fig. 1(c) exhibit diffraction peaks at 2θ = 38.13°, 44.28°, 64.75°, and 77.70°, corresponding to the (111), (200), (220), and (311) planes of face-centered cubic Au, respectively (Goudeli et al. 2017). The high crystallinity index of 98.75% indicates the highly crystalline nature of the synthesized AuNP.

For the TiO_2@COF-5 composite in Fig. 1(d), the diffraction peaks at 2θ = 3.04°, 5.98°, 6.68°, and 9.11° are associated with the COF-5 framework, while the peaks at 25.23° and 47.93° correspond to the anatase TiO_2 phase. The coexistence of these characteristic peaks confirms the successful formation of the TiO_2@COF-5 composite. The decrease in crystallinity index to 47.53% may be attributed to partial structural disorder or interfacial interactions between TiO_2 and the COF-5 framework. Similarly, the XRD pattern of AuNP@COF-5 in Fig. 1(e) shows the characteristic low-angle peaks of COF-5 and the fcc Au reflections at 37.41°, 44.70°, 64.51°, and 77.55°. These results confirm the successful incorporation of AuNPs into the COF-5 structure while largely retaining the ordered framework, as reflected by its crystallinity index of 66.49%.

The HR-TEM, SAED, and EDX analyses provide consistent evidence for the successful incorporation of AuNPs into the COF-5 framework, as shown in Fig. 2(a–c). In the HR-TEM image, the COF-5 matrix appears as a low-contrast sheet-like structure, while AuNPs are observed as dark nanodomains due to the high electron density of gold. These AuNPs are closely associated with the COF-5 matrix and exhibit nearly spherical morphology, although several particles appear in close contact, suggesting partial agglomeration during synthesis or sample preparation. The crystalline nature of AuNPs is further confirmed by the SAED pattern in Fig. 2(b), which shows distinct bright diffraction spots superimposed on a diffuse halo from the COF-5 matrix. In addition, the EDX result in Fig. 2(c) verifies the elemental composition of the composite, showing dominant C and O signals of 74.91 and 24.88 at.%, respectively, together with a small but detectable Au signal of 0.21 at.%. The low Au content indicates that AuNPs are present as a minor phase in the analyzed region, but their incorporation is supported by both the high-contrast domains observed in HR-TEM and the Au signal detected by EDX. SEM analysis in Fig. S1 also shows an increase in particle size from 6.23–12.47 nm for COF-5 to 8.08–16.18 nm for COF-5@AuNP, indicating morphological changes and partial aggregation after composite formation.

A comparable structural confirmation is obtained for TiO_2@COF-5, as presented in Fig. 2(d–f). The HR-TEM image in Fig. 2(d) reveals darker TiO_2 domains distributed on the low-contrast COF-5 matrix, indicating close contact between TiO_2 particles and the COF-5 framework. The TiO_2 particles show rounded to polyhedral morphology and tend to form clustered domains, suggesting partial aggregation on the COF-5 surface. At higher magnification, visible lattice fringes are observed in the TiO_2 region, confirming that TiO_2 maintains its crystalline structure after composite formation. This result is supported by the SAED pattern in Fig. 2(e), which displays bright diffraction rings and spots corresponding to crystalline TiO_2, along with a diffuse background attributed to the COF-5 matrix. The EDX analysis in Fig. 2(f) further confirms the presence of C, O, and Ti with atomic fractions of 13.28, 42.07, and 44.65 at.%, respectively. The high Ti and O contents indicate that TiO_2 is the dominant inorganic phase in the analyzed area, while the C signal confirms the contribution of the COF-5 framework. Consistent with these observations, SEM analysis in Fig. S1 shows a slight increase in particle size from 5.62–11.25 nm for TiO_2 to 6.20–12.40 nm for TiO_2@COF-5, reflecting morphological changes associated with TiO_2 attachment and clustering on the COF-5 matrix.

3.2. XPS Analysis of COF-5, AuNP@COF-5 and TiO_2@COF-5

XPS analysis was used to evaluate the surface composition of COF-5, AuNP@COF-5, and TiO_2@COF-5. The XPS spectrum of pristine COF-5 shows the characteristic signals of C 1s, O 1s, and B 1s, as shown in Fig. S2, confirming the presence of a carbon-rich framework, oxygen-containing linkage environment, and boron-containing units. This result is consistent with the composition of borate/boronate ester-based COFs, as discussed by Li et al., where the framework is mainly composed of carbon-, oxygen-, and boron-containing structural units (Li et al. 2024).

After the incorporation of AuNPs or TiO_2, the XPS quantification results summarized in Table S1 (refer to the supplementary file) show that both composites are still dominated by carbon and oxygen, indicating that COF-5 remains the major surface component. For AuNP@COF-5, the weak Au contribution observed by XPS is consistent with the EDX result in Fig. 2(c), where Au was detected as a minor component together with dominant C and O signals. This agreement supports the successful incorporation of AuNPs into the COF-5 matrix at a relatively low amount, as evidenced by the dark AuNP domains in HR-TEM. The low Au signal may be associated with the small amount of AuNPs introduced during synthesis, high dispersion, partial embedding within the COF-5 pores, or surface coverage by the framework. Similar behavior was reported by Pachfule et al., who showed that Au nanoparticles could be immobilized within a stable COF matrix to form Au–COF hybrids for the reduction of nitrophenol (Pachfule, P.; Kandambeth, S.; Díaz, D. D.; Banerjee 2014). Zhang et al. also demonstrated that highly dispersed Au nanoparticles can be anchored on a modified COF support, where the Au signal verifies the incorporation of Au species into the COF-based structure (Zhang et al. 2020).

For TiO_2@COF-5, the presence of Ti 2p confirms the successful introduction of TiO_2 into the COF-5 matrix. This result is consistent with the HR-TEM and SAED observations in Fig. 2(d,e), where crystalline TiO_2 domains were observed on the COF-5 matrix, as well as the EDX result in Fig. 2(f), which shows clear Ti and O contributions in the composite. The lower Ti contribution in XPS compared with the Ti-rich EDX region suggests that TiO_2 is successfully incorporated but may not be uniformly exposed across the outer surface. Some TiO_2 domains may be partially covered by or embedded within the COF-5 matrix, consistent with the clustered TiO_2 morphology observed in HR-TEM. This interpretation aligns with TiO_2/COF composite studies, in which the detection of Ti alongside framework elements supports the formation of TiO_2–COF hybrid photocatalysts (Yao et al. 2024; Xue et al. 2024).

The narrow-scan XPS results further provide information on the local oxygen environments in the composites as observed in Fig. 3. In AuNP@COF-5, the O 1s signal is mainly associated with oxygen-containing environments in the COF-5 framework, particularly boronate ester-related oxygen, with possible contributions from residual oxygen-containing groups and adsorbed oxygen species. The presence of Au 4f supports the incorporation of Au species. However, its low intensity is consistent with the minor Au contribution observed by EDX and the high-contrast AuNP domains in HR-TEM. In TiO_2@COF-5, the O 1s signal arises from overlapping oxygen environments of COF-5 and TiO_2, including framework oxygen, Ti–O-related oxygen, surface hydroxyl groups, and adsorbed oxygen species. The presence of Ti 2p further confirms the incorporation of TiO_2 into the COF-5 structure. The broad O 1s profiles observed in both composites indicate multiple oxygen environments, suggesting that oxygen-containing sites of COF-5 remain involved after AuNP or TiO_2 incorporation and may contribute to interfacial interaction between the framework and the inorganic components.

3.3. Photodegradation of 4-Nitrophenol

Photodegradation was evaluated using three kinetic models: the modified pseudo-first-order (PFO), pseudo-second-order (PSO), and biphasic first-order models. These models are widely used to describe

degradation kinetics and provide insight into the apparent reaction rate and kinetic behavior of photocatalytic systems, particularly during the early stages of the reaction. The use of PFO-type kinetics in photocatalytic degradation is commonly associated with the Langmuir–Hinshelwood approximation under low pollutant concentration conditions (Tran et al. 2023).

Photodegradation efficiency is highly dependent on the ability of photogenerated charge carriers to participate effectively in redox reactions. The generation, separation, and transfer of electron–hole pairs are therefore critical factors governing the overall degradation performance. Limitations, such as rapid charge recombination or inefficient interfacial charge transfer, may decrease the reaction rate and lead to deviations from ideal single-step kinetic behavior.

In this study, the kinetic analysis was performed using the normalized degradation fraction of 4-nitrophenol (4-NP), expressed as:

$$X_t = \frac{C_o - C_t}{C_o}$$

1

where C_o is the initial 4-NP concentration and C_t is the remaining 4-NP concentration at irradiation time t. The experimental data were fitted using modified PFO, PSO, and biphasic first-order kinetic models to determine the apparent rate constants and evaluate the most suitable kinetic model for describing the 4-NP photodegradation process. The modified PFO and PSO equations were adapted from the nonlinear pseudo-order kinetic expressions described in (Angela et al. 2021). while the biphasic first-order model was adopted based on the double first-order in parallel (DFOP) concept, which represents degradation as the sum of two first-order processes with different rate constants (NAFTA 2011). The DFOP (bi-exponential) model has been recommended for degradation profiles that deviate from single first-order behavior, particularly when a rapid initial stage is followed by a slower degradation stage (FOCUS 2006). The equations are expressed as follows:

$$X_t = A(1 - \exp(-k_1 t))$$

2

$$X_t = \frac{A^2 k_2 t}{1 + A k_2 t} \qquad (3)$$

$$X_t = A_1\left(1 - \exp\left(-k_f t\right)\right) + A_2\left(1 - \exp\left(-k_s t\right)\right) \qquad (4)$$

where X_t represents the normalized degradation fraction at irradiation time t, A is the apparent maximum degradation fraction in the modified PFO and PSO models, A_1 and A_2 represent the fractional contributions of the fast and slow degradation stages, respectively. The sum A_1+ A_2 corresponds to the overall apparent maximum degradation fraction. The parameters k_1, k_2, k_f, and k_s

are the modified PFO rate constant, PSO rate constant, fast-stage first-order rate constant, and slow-stage first-order rate constant, respectively. Since the kinetic models were fitted using the dimensionless normalized degradation fraction X_t, the parameters A, A_1 and A_2 are dimensionless, while all rate constants (k_1, k_2, k_f, and k_s) are expressed in min^{-1}. The biphasic first-order model was included to account for the non-single-exponential behavior observed in the degradation profiles, particularly the rapid initial increase followed by a slower subsequent stage during prolonged irradiation.

The photodegradation kinetics of 4-NP in Fig. 4 showed that TiO_2@COF-5 was the most effective photocatalyst under UV irradiation, followed by AuNP@COF-5, TiO_2, AuNP, and COF-5. The superior activity of TiO_2@COF-5 can be attributed to the synergistic interaction between the UV-responsive TiO_2 phase and COF-5, which serves as a porous support that promotes particle dispersion, active-site accessibility, and interfacial interactions with 4-NP molecules. This interpretation is consistent with the general characteristics of COF-based photocatalysts, which are attractive for photocatalysis because of their structural regularity, robust frameworks, inherent porosity, and photocatalytic activity. Wang et al. reported that COFs and COF-based photocatalysts have been extensively investigated because of their ordered structures and porous frameworks, which are beneficial for photocatalytic applications (Wang et al. 2020). Yang et al. also emphasized that COFs possess large surface areas, tunable pore sizes, π-conjugated structures, and chemical stability, which make them promising photocatalysts for water splitting, dye degradation, CO_2 reduction, and organic synthesis (Yang et al. 2020).

The enhanced activity of TiO_2@COF-5 relative to pristine TiO_2 is consistent with reports on COF-based composites, in which coupling COFs with semiconductor photocatalysts improves photocatalytic performance through stronger interfacial contact, enhanced charge separation, and broader interaction with pollutant molecules. Hu et al. summarized that effective strategies for improving COF-based photodegradation include ligand and structural design as well as the construction of COF composites with MOFs, g-C_3N_4, and metal semiconductors (Hu et al. 2022). In addition, the crystallinity of COFs has been reported to influence light harvesting, charge separation, and charge transfer, which are key factors in photocatalytic performance (Mishra et al. 2023). These findings support the interpretation that COF-5 contributes not merely as a passive support but as a porous matrix that improves the accessibility and interfacial efficiency of TiO_2 during 4-NP photodegradation.

For AuNP@COF-5, the higher activity compared with AuNPs alone indicates that COF-5 also enhances AuNP performance by improving dispersion and facilitating interfacial charge-transfer processes. Under the UV irradiation, however, AuNPs are more appropriately considered as charge-transfer mediators or electron-trapping sites rather than the primary photocatalytic component. This interpretation aligns with reports on COF-based composite photocatalysts, where combining COFs with other active components can enhance charge separation and photocatalytic efficiency via interfacial interactions. Therefore, although AuNP@COF-5 showed better activity than AuNP, TiO_2@COF-5 remained superior because TiO_2 is more directly activated under UV irradiation.

The modified PFO and PSO models described the general degradation trend, with R^2 values of approximately 0.67–0.85 and 0.83–0.95, respectively. The better fitting quality of the PSO model suggests that surface interactions among 4-NP, reactive species, and photocatalytic active sites contributed to the degradation process. Nevertheless, the biphasic first-order model provided the best fit for all materials, with R^2 values of approximately 0.98–0.99, indicating that the degradation profiles did not follow single-exponential behavior. Similar two-step kinetic behavior has been reported in photocatalytic systems; for example, Sahu and Das observed that Ag_2O-impregnated ZnO nanorods exhibited two-step visible-light photocatalytic degradation of methylene blue, whereas pristine ZnO followed a single-slope pseudo-first-order profile (Sahu et al. 2022). The two kinetic regions in the Ag_2O/ZnO heterostructure were attributed to the synergistic interaction between Ag_2O and ZnO during photocatalysis. In another heterostructured photocatalytic system, Das et al. reported bi-phasic dye-degradation behavior for ZnO/Ag_2O/g-C_3N_4 composite heterostructures, where the heterojunction structure and metallic Ag contributed to enhanced charge separation and improved photocatalytic activity (Das et al. 2024). These reports support the interpretation that the COF-5-based composites in the present work involve more than one kinetic regime during 4-NP photodegradation. In addition, Wilde et al. applied pseudo- and biphasic first-order kinetics to pollutant degradation in hospital wastewater and found that biphasic fitting was more appropriate when the degradation profile included a rapid initial stage followed by a slower stage (Wilde et al. 2014). Although their system was based on ozonation rather than photocatalysis, their kinetic treatment supports the use of a biphasic model for degradation processes that deviate from single first-order behavior.

The biphasic parameters further clarify the contribution of the fast and slow degradation stages for each material. TiO_2@COF-5 exhibited a dominant fast phase, as indicated by $A_1 = 0.62$ with $k_f = 0.24$/min, suggesting that a major fraction of 4-NP degradation occurred during the early irradiation period. In the slow phase, $A_2 = 0.38$ and ks = 0.03/min indicate that degradation continued at longer irradiation times, albeit at a lower rate. AuNP@COF-5 also showed two-stage behavior, with $A_1 = 0.59$ and $k_f = 1.30$/min for the fast phase and $A_2 = 0.41$ and $k_s = 0.02$/min for the slow phase. Although AuNP@COF-5 exhibited a higher k_f, TiO_2@COF-5 showed a greater fast-phase contribution and higher final degradation performance. This suggests that photocatalytic activity is governed not only by the magnitude of the rate constant, but also by the relative contribution of each kinetic stage during irradiation.

3.4. Photodegradation Mechanism

The combined action of UV irradiation, H_2O_2, and the photocatalysts drives the photodegradation in this study. Under UV light, the photocatalyst generates electron–hole pairs, where conduction-band electrons reduce dissolved oxygen to $O_2^{\bullet -}$, while valence-band holes oxidize water or hydroxide species to •OH. This mechanism follows the general principle of semiconductor photocatalysis, in which photogenerated charge carriers initiate the formation of reactive oxygen species (ROS) that degrade pollutants (Hoffmann et al. 1995; Nosaka et al. 2016). The addition of H_2O_2 further promotes •OH formation through UV photolysis and electron-assisted reactions, while also acting as an electron acceptor that

suppresses electron–hole recombination. However, excessive H_2O_2 may reduce degradation efficiency because it can scavenge •OH to form HO_2•, which has lower oxidative ability than •OH (Yao et al. 2013). Therefore, the efficiency of 4-NP degradation depends on the balance between ROS generation, charge separation, and radical scavenging.

In COF-5-based systems, the framework enhances local interactions between 4-NP and the active species. The COF-5 structure provides accessible sites that can concentrate 4-NP, H_2O_2, and dissolved oxygen near the photocatalytic centers, thereby increasing the probability of ROS attack. This role aligns with reports that COF-based materials can improve photocatalytic pollutant degradation through molecular accessibility, surface interactions, and charge-transfer pathways (Hu et al. 2022). In COF-5@TiO_2, TiO_2 serves as the main UV-active component for electron–hole generation, while COF-5 supports substrate accessibility and interfacial interaction. In AuNP@COF-5, AuNPs can act as electron sinks that facilitate electron transfer and reduce recombination, as noble-metal modification has been reported to improve photocatalytic efficiency by prolonging charge-carrier lifetime (Pellegrino et al. 2017).

A critical limitation in this study is that the catalyst was present in a dissolved or highly dispersed condition during the photodegradation process. Therefore, the observed degradation cannot be assigned solely to a conventional heterogeneous surface mechanism. Instead, the reaction should be interpreted as a mixed heterogeneous–quasi-homogeneous photocatalytic process, in which ROS are generated both on the catalyst surface and by dispersed catalytic species in solution. This condition may increase the apparent degradation efficiency by improving contact among 4-NP, H_2O_2, dissolved oxygen, UV light, and ROS, but it also limits the interpretation of intrinsic catalyst activity, structural stability, recoverability, and reusability.

The dissolved or highly dispersed catalyst state can be explained by the aqueous UV/H_2O_2 environment and the materials' structural nature as shown in Fig. 5. COF-5 is a boronate ester-linked COF, and boronate ester bonds are known to be vulnerable to hydrolysis because water can attack electron-deficient boron centers, weakening the framework under aqueous conditions (Li et al. 2018). Smith et al. (2015) also showed that the water stability of boronate ester-linked COFs strongly depends on framework structure and reaction environment (Smith et al. 2015). In TiO_2-containing systems, nanoparticles can remain as fine aqueous suspensions and exhibit dispersion–aggregation behavior during photocatalysis, thereby affecting light absorption, scattering, and catalytic performance (Tolosana-Moranchel et al. 2021). For AuNP-containing systems, weak attachment between AuNPs and the COF matrix may promote redistribution of nanoparticles in the reaction medium, making the activity dependent not only on fixed interfacial sites but also on dispersed metal-containing species.

The transformation of 4-NP mainly proceeds through radical-mediated oxidation. Hydroxyl radicals attack the aromatic ring and the nitro-substituted structure of 4-NP, forming hydroxylated intermediates such as 4-nitrocatechol and further-oxidized products, consistent with the UV/H_2O_2 degradation pathway of 4-NP reported by (Daneshvar et al. 2007). The detection of 4-aminophenol should be interpreted as a

parallel reductive pathway involving photogenerated electrons and protons, because the conversion of $–NO_2$ to $–NH_2$ requires reduction rather than direct oxidation by •OH. However, the decreasing absorbance around 300 nm suggests that 4-AP did not accumulate as a stable final product, but was also transformed further under the UV/H_2O_2/photocatalyst system (refer to Fig. S4). Thus, the overall 4-NP transformation involves both oxidative photodegradation and reductive photocatalytic conversion, followed by further degradation of intermediate products. This process is controlled by ROS availability, electron transfer, H_2O_2 concentration, oxygen availability, and the dispersed catalyst condition in solution.

4. Conclusion

COF-5, TiO_2@COF-5, and AuNP@COF-5 were successfully synthesized and applied for the photodegradation of 4-nitrophenol under UV/H_2O_2 irradiation. XRD, HR-TEM, SAED, EDX, and XPS analyses confirmed the formation of the COF-5 framework and the successful incorporation of TiO_2 or AuNP into the composite structures. The photocatalytic activity followed the order: TiO_2@COF-5 > AuNP@COF-5 > TiO_2 > AuNP > COF-5, indicating that the COF-5-TiO_2 modification provided the most effective system for 4-NP degradation. The superior performance of TiO_2@COF-5 was attributed to TiO_2 as the main UV-active component and to COF-5 as a porous framework that improved substrate accessibility, particle dispersion, and interfacial interactions. Kinetic analysis showed that the biphasic first-order model gave the best fit, with R^2 values of approximately 0.98–0.99, suggesting that 4-NP degradation occurred through a rapid initial stage followed by a slower stage. The degradation process was governed by ROS generation, electron transfer, and further transformation of intermediate products, including the parallel formation and subsequent degradation of 4-aminophenol. However, because the catalyst was present in a dissolved or highly dispersed condition during the reaction, the process should be interpreted as a mixed heterogeneous–quasi-homogeneous photocatalytic system rather than a purely heterogeneous surface reaction. Overall, TiO_2@COF-5 showed the most promising performance for the degradation of nitroaromatic pollutants, although further improvements in catalyst stability, recoverability, and reusability are still required.

Declarations

Ethical Approval

Not applicable. This study did not involve human participants, animals, or clinical samples.

Consent to Participate

Not applicable. This study did not involve human participants.

Consent to Publish

Not applicable. This manuscript does not contain any individual person's data, images, or identifiable information.

Declarations of Generative AI and AI-assisted technologies in the writing process

During the preparation of this work, the author(s) used generative artificial intelligence (AI), such as Google Gemini, to improve clarity and grammar, search for journals, and sharpen the visualization of analysis results. The AI tool/service was not used to generate original scientific content, interpret results, or draw conclusions. All ideas, analyses, and findings presented in this work are the responsibility of the authors. The authors have carefully reviewed and edited the output generated by AI tool/service to ensure its accuracy and integrity.

Declaration of competing interest

The authors declare that they have no known competing financial interests or personal relationships that could have influenced the work reported in this paper.

Funding

The authors received no financial support for the research, authorship, and/or publication of this article.

Authors' Contributions

Conceptualization: KJ Imanuela, R Sanjaya, JN Putro; Methodology: KJ Imanuela, R Sanjaya; Formal analysis and investigation: KJ Imanuela, R Sanjaya, A Rahmawati, A Kurniawan; Writing - original draft preparation: KJ Imanuela, R Sanjaya; Writing - review and editing: JN Putro, S Ismadji; Resources: A Kurniawan, O Shimomura; Supervision: JN Putro, S Ismadji

Acknowledgements

Not applicable.

Data availability

Data will be available on request.

References

1. Angela S, Bervia Lunardi V, Kusuma K, Edi Soetaredjo F, Nyoo Putro J, Permatasari Santoso S, Elisa Angkawijaya A, Lie J, Gunarto C, Kurniawan A, Ismadji S (2021) Facile synthesis of hierarchical porous ZIF-8@TiO2 for simultaneous adsorption and photocatalytic decomposition of crystal violet. Environ Nanotechnol Monit Manag 16. https://doi.org/10.1016/j.enmm.2021.100598
2. Basuki TM, Indrawati DR, Nugroho HYSH, Pramono IB, Setiawan O, Nugroho NP, Nada FMH, Nandini R, Savitri E, Adi RN, Purwanto P, Sartohadi J (2024) Water Pollution of Some Major Rivers in Indonesia: The Status, Institution, Regulation, and Recommendation for Its Mitigation. Pol J Environ Stud 33:3515–3530. https://doi.org/10.15244/pjoes/178532
3. Bi S (2022) Photoredox Catalysis by Covalent Organic Frameworks. In: Gao Y, Lu F (eds) Covalent Organic Frameworks. IntechOpen, London. https://doi.org/10.5772/intechopen.107485
4. Bilal M, Bagheri AR, Bhatt P, Chen S (2021) Environmental occurrence, toxicity concerns, and remediation of recalcitrant nitroaromatic compounds. J Environ Manag 291:112685. https://doi.org/10.1016/j.jenvman.2021.112685
5. Côté AP, Benin AI, Ockwig NW, O'Keeffe M, Matzger AJ, Yaghi OM (2005) Porous, crystalline, covalent organic frameworks. Science 310:1166–1170. https://doi.org/10.1126/science.1120411
6. Daneshvar N, Behnajady MA, Zorriyeh Asghar Y (2007) Photooxidative degradation of 4-nitrophenol (4-NP) in UV/H2O2 process: Influence of operational parameters and reaction mechanism. J Hazard Mater 139:275–279. https://doi.org/10.1016/j.jhazmat.2006.06.045
7. Das D, Sahu P (2024) ZnO/Ag2O/g-C3N4 composite heterostructures with Ag0-induced superior visible light photocatalytic activity via unique bi-phasic dye-degradation phenomena. Opt Mater 147:114596. https://doi.org/10.1016/J.OPTMAT.2023.114596
8. North American Free Trade Agreement (NAFTA) Technical Working Group on Pesticides (2011) Guidance for evaluating and calculating degradation kinetics in environmental media. https://www.epa.gov/sites/default/files/2015-09/documents/degradation-kin.pdf. Accessed 3 Jun 2026
9. FOrum for the Co-ordination of pesticide fate models and their USe (FOCUS), Work Group on Degradation Kinetics (2006) Guidance document on estimating persistence and degradation kinetics from environmental fate studies on pesticides in EU registration. EC Document Reference SANCO/10058/2005, version 2.0, 434 pp
10. Goudeli E, Pratsinis SE (2017) Surface Composition and Crystallinity of Coalescing Silver–Gold Nanoparticles. ACS Nano 11:11653–11660. https://doi.org/10.1021/acsnano.7b06727
11. Gu Y, Li S, Li M, Wang X, Liu Y, Shi K, Bai X, Yao Q, Wu Z, Yao H (2023) Recent advances in g-C 3 N 4 -based photo-enzyme catalysts for degrading organic pollutants. RSC Adv 13:937–947. https://doi.org/10.1039/D2RA06994F
12. Hoffmann MR, Martin ST, Choi W, Bahnemann DW (1995) Environmental Applications of Semiconductor Photocatalysis. Chem Rev 95:69–96. https://doi.org/10.1021/cr00033a004
13. Hu S-Y, Sun Y-N, Feng Z-W, Wang F-O, Lv Y (2022) Design and construction strategies to improve covalent organic frameworks photocatalyst's performance for degradation of organic pollutants.

Chemosphere 286:131646. https://doi.org/10.1016/j.chemosphere.2021.131646

14. Khan KO, Assiri MA, Irshad H, Rafique S, Khan AM, Khan AK, Imran M, Shahzad SA (2023) Fluorescence based detection of industrially important and hazardous 4-Nitrophenol in real Samples: A combination of Extensive optical and theoretical studies. J Photochem Photobiol Chem. https://doi.org/10.1016/j.jphotochem.2023.114805. 442:
15. Li H, Li H, Dai Q, Li H, Brédas J (2018) Hydrolytic Stability of Boronate Ester-Linked Covalent Organic Frameworks. Adv Theory Simul 1:1700015. https://doi.org/10.1002/adts.201700015
16. Li X, Jin X, Ma L, Ma X, Zhang Q, Bai H, Ma Y, Li Y, Chen W, She M (2024) Construction of borate-ester-based COFs with high specific surface area for the detection of H2O content in the food field. Microchem J 199:109976. https://doi.org/10.1016/J.MICROC.2024.109976
17. Mishra B, Alam A, Kumbhakar B, Díaz Díaz D, Pachfule P (2023) Impact of the Crystallinity of Covalent Organic Frameworks on Photocatalytic Hydrogen Evolution. Cryst Growth Des 23:4701–4719. https://doi.org/10.1021/acs.cgd.3c00379
18. Nosaka Y, Nosaka A (2016) Understanding Hydroxyl Radical (• OH) Generation Processes in Photocatalysis. ACS Energy Lett 1:356–359. https://doi.org/10.1021/acsenergylett.6b00174
19. Pachfule P, Kandambeth S, Díaz DD, Banerjee R (2014) Highly stable covalent organic framework–Au nanoparticles hybrids for enhanced activity for nitrophenol reduction. Chem Commun 50:3169–3172. https://doi.org/10.1039/C3CC49176E
20. Pellegrino F, Pellutiè L, Sordello F, Minero C, Ortel E, Hodoroaba VD, Maurino V (2017) Influence of agglomeration and aggregation on the photocatalytic activity of TiO2 nanoparticles. Appl Catal B Environ 216:80–87. https://doi.org/10.1016/j.apcatb.2017.05.046
21. Ritchie LK, Trewin A, Reguera-Galan A, Hasell T, Cooper AI (2010) Synthesis of COF-5 using microwave irradiation and conventional solvothermal routes. Microporous Mesoporous Mater 132:132–136. https://doi.org/10.1016/j.micromeso.2010.02.010
22. Sahu P, Das D (2022) Two-Step Visible Light Photocatalytic Dye Degradation Phenomena in Ag2O-Impregnated ZnO Nanorods via Growth of Metallic Ag and Formation of ZnO/Ag0/Ag2O Heterojunction Structures. Langmuir 38:4503–4520. https://doi.org/10.1021/acs.langmuir.1c02860
23. Smith BJ, Dichtel WR (2014) Mechanistic studies of two-dimensional covalent organic frameworks rapidly polymerized from initially homogenous conditions. J Am Chem Soc 136:8783–8789. https://doi.org/10.1021/ja5037868
24. Smith BJ, Hwang N, Chavez AD, Novotney JL, Dichtel WR (2015) Growth rates and water stability of 2D boronate ester covalent organic frameworks. Chem Commun 51:7532–7535. https://doi.org/10.1039/c5cc00379b
25. Tiwari J, Tarale P, Sivanesan S, Bafana A (2019) Environmental persistence, hazard, and mitigation challenges of nitroaromatic compounds. Environ Sci Pollut Res 26:28650–28667. https://doi.org/10.1007/s11356-019-06043-8
26. Tolosana-Moranchel A, Pecharromán C, Faraldos M, Bahamonde A (2021) Strong effect of light scattering by distribution of TiO2 particle aggregates on photocatalytic efficiency in aqueous

suspensions. Chem Eng J 403:126186. https://doi.org/10.1016/J.CEJ.2020.126186

27. Tran HD, Nguyen DQ, Do PT, Tran UNP (2023) Kinetics of photocatalytic degradation of organic compounds: a mini-review and new approach. RSC Adv 13:16915–16925. https://doi.org/10.1039/D3RA01970E
28. Turkevich J, Stevenson PC, Hillier J (1951) A study of the nucleation and growth processes in the synthesis of colloidal gold. Discuss Faraday Soc 11:55–75. https://doi.org/10.1039/df9511100055
29. Utami RR, Geerling GW, Salami IRS, Notodarmojo S, Ragas AMJ (2020) Environmental prioritization of pesticide in the Upper Citarum River Basin, Indonesia, using predicted and measured concentrations. Sci Total Environ 738:140130. https://doi.org/10.1016/j.scitotenv.2020.140130
30. Wang H, Wang H, Wang Z, Tang L, Zeng G, Xu P, Chen M, Xiong T, Zhou C, Li X, Huang D, Zhu Y, Wang Z, Tang J (2020) Covalent organic framework photocatalysts: structures and applications. Chem Soc Rev 49:4135–4165. https://doi.org/10.1039/D0CS00278J
31. Wilde ML, Montipó S, Martins AF (2014) Degradation of β-blockers in hospital wastewater by means of ozonation and Fe2+/ozonation. Water Res 48:280–295. https://doi.org/10.1016/J.WATRES.2013.09.039
32. Xue R, Liu Y, Wu X, Lv Y, Guo J, Yang G-Y (2024) Covalent Organic Frameworks Meet Titanium Oxide. ACS Nano 18:19443–19469. https://doi.org/10.1021/acsnano.4c06845
33. Yaacob N, Ismail AF, Sean GP, Nazri NAM (2019) Structural and photocatalytic properties of co-doped hybrid ZrO2–TiO2 photocatalysts. SN Appl Sci 1:252. https://doi.org/10.1007/s42452-019-0247-4
34. Yadav V, Verma P, Negi H, Singh RK, Saini VK (2023) Efficient degradation of 4-nitrophenol using VO(TPP) impregnated TiO2 photocatalyst: Insight into kinetics and mechanism. J Mater Res 38:237–247. https://doi.org/10.1557/s43578-022-00856-z
35. Yang Q, Luo M, Liu K, Cao H, Yan H (2020) Covalent organic frameworks for photocatalytic applications. Appl Catal B Environ 276:119174. https://doi.org/10.1016/j.apcatb.2020.119174
36. Yao D, Xie X, Liang X, Lu S, Lai H (2024) Photocatalytic Degradation of Malachite Green by Titanium Dioxide/Covalent Organic Framework Composite: Characterization, Performance and Mechanism. ChemistryOpen 13:e202300209. https://doi.org/10.1002/open.202300209
37. Yao H, Sun P, Minakata D, Crittenden JC, Huang C-H (2013) Kinetics and Modeling of Degradation of Ionophore Antibiotics by UV and UV/H2O2. Environ Sci Technol 47:4581–4589. https://doi.org/10.1021/es3052685
38. Zhang Q-P, Sun Y, Cheng G, Wang Z, Ma H, Ding S-Y, Tan B, Bu J, Zhang C (2020) Highly dispersed gold nanoparticles anchoring on post-modified covalent organic framework for catalytic application. Chem Eng J 391:123471. https://doi.org/10.1016/j.cej.2019.123471
39. Zhou L, Huang Z, Zhang H, Gao H, Tang J, Yao X (2023) Construction of a Novel TiO2-Covalent-Organic-Framework Heterojunction for Highly Selective Photo-Oxidation Coupling of Amines under Visible Light Irradiation. ChemCatChem 15:e202300414. https://doi.org/10.1002/cctc.202300414

Figures

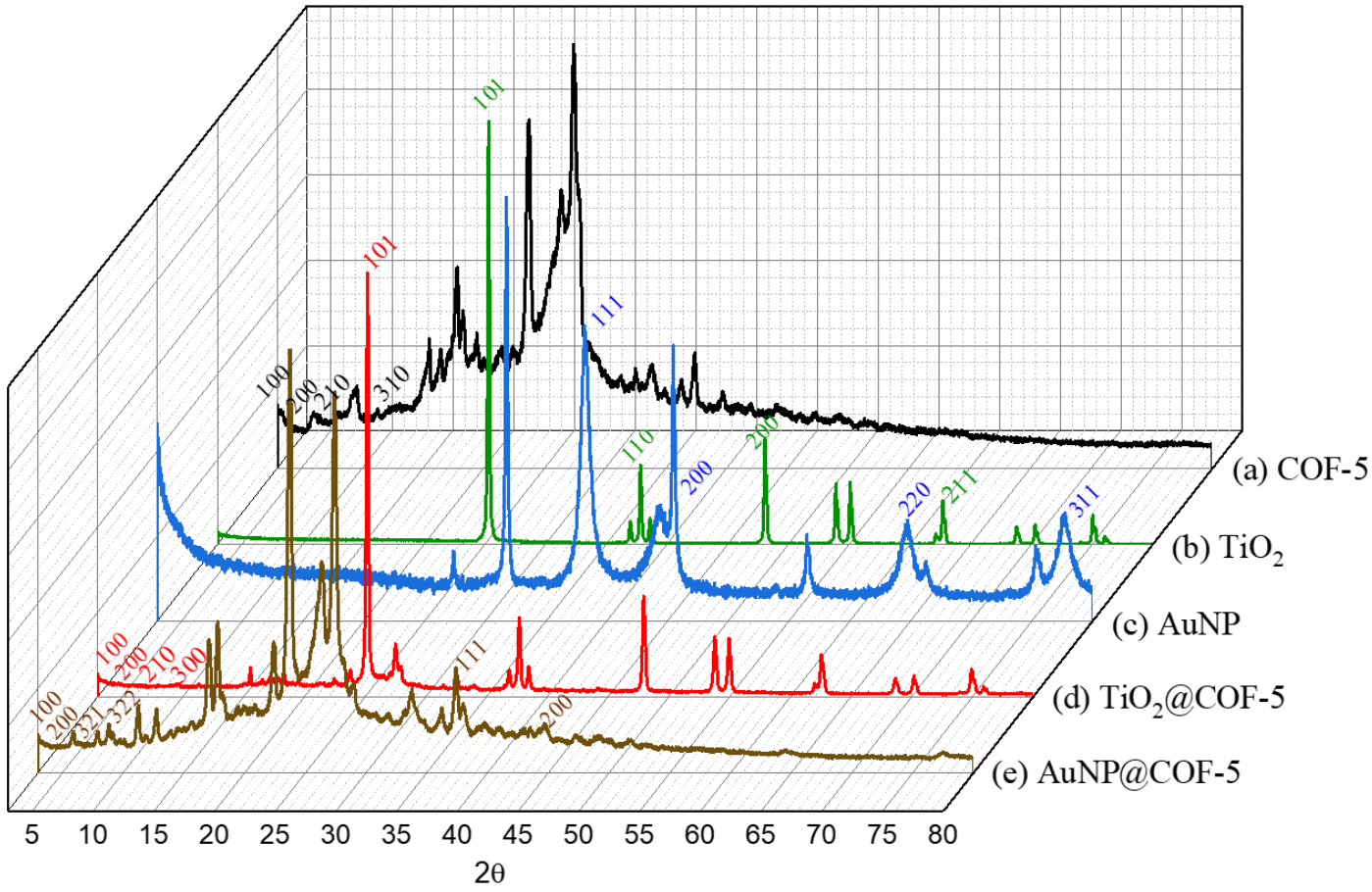

Figure 1

XRD pattern of the photocatalysts

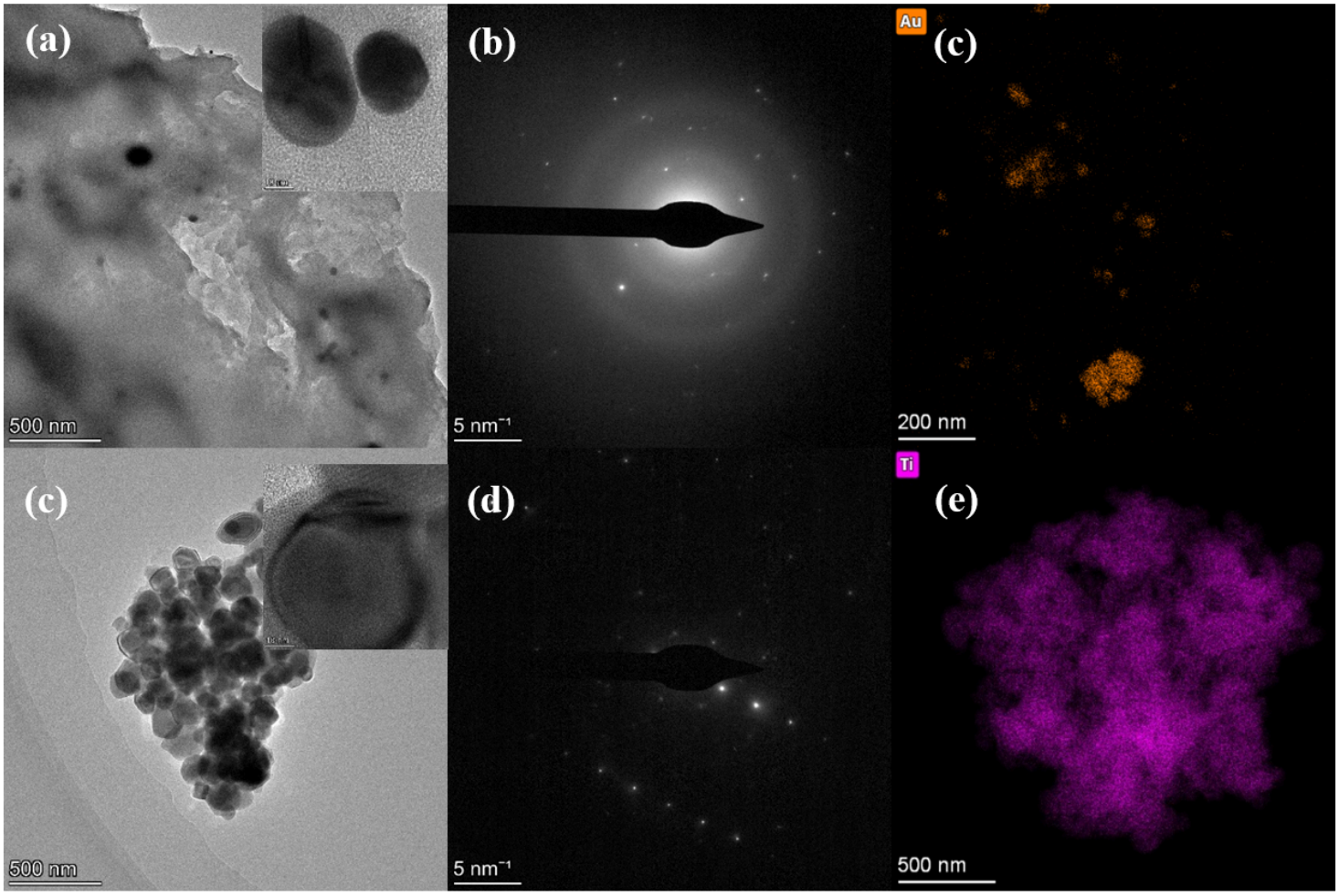

Figure 2

HR-TEM, SAED, and EDX of (a-c) AuNP@COF-5 and (d-e) TiO_2@COF-5 composites

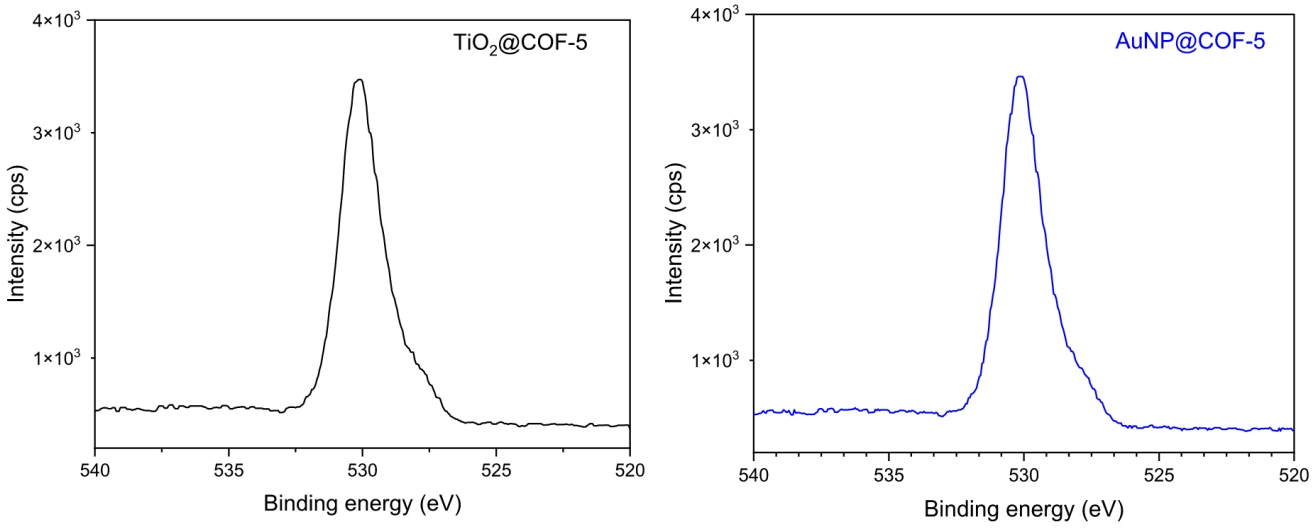

Figure 3

XPS spectra of AuNP@COF-5 (right) and TiO_2@COF-5 (left)

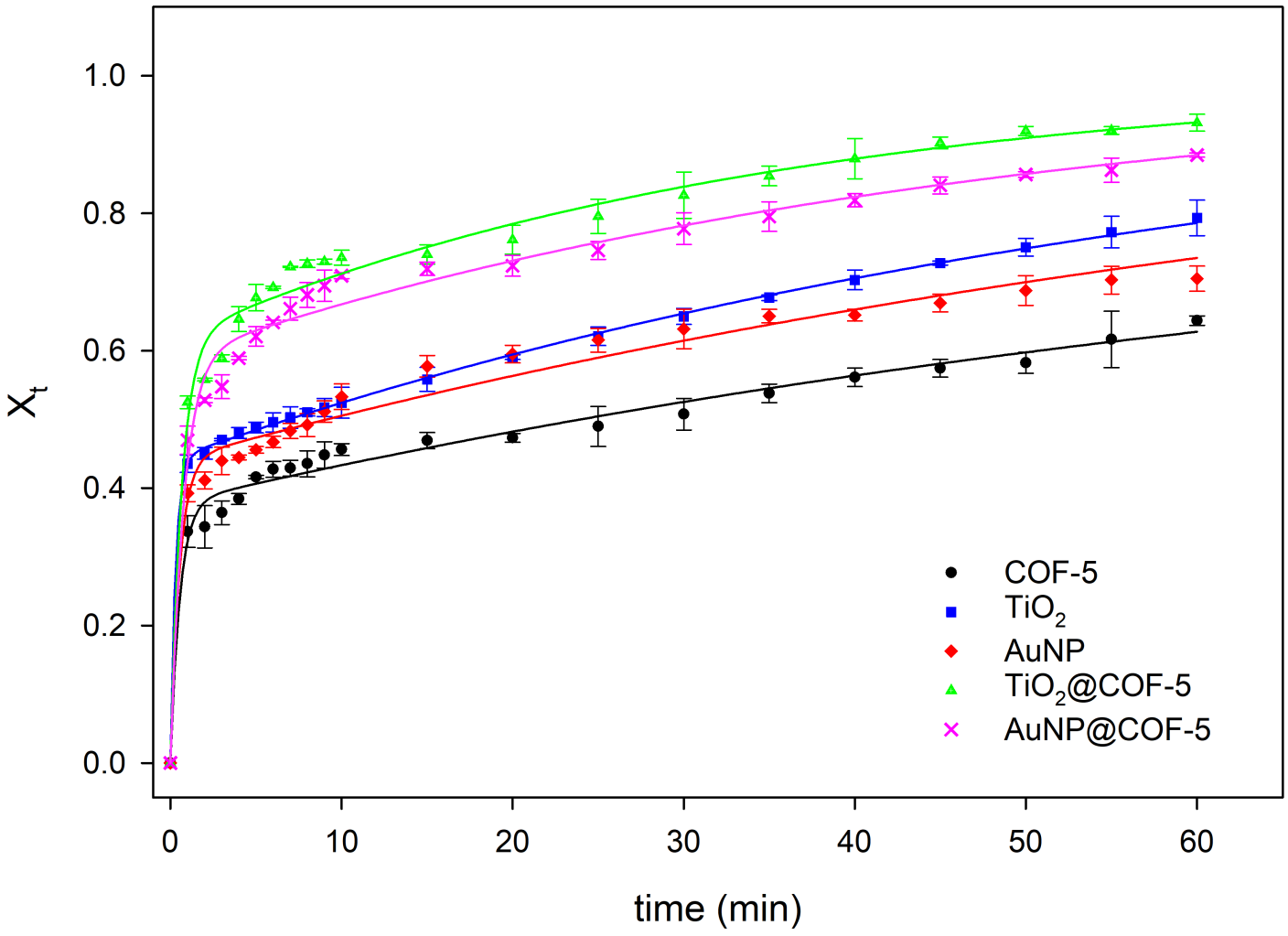

Figure 4

Photodegradation Kinetics of 4-NP

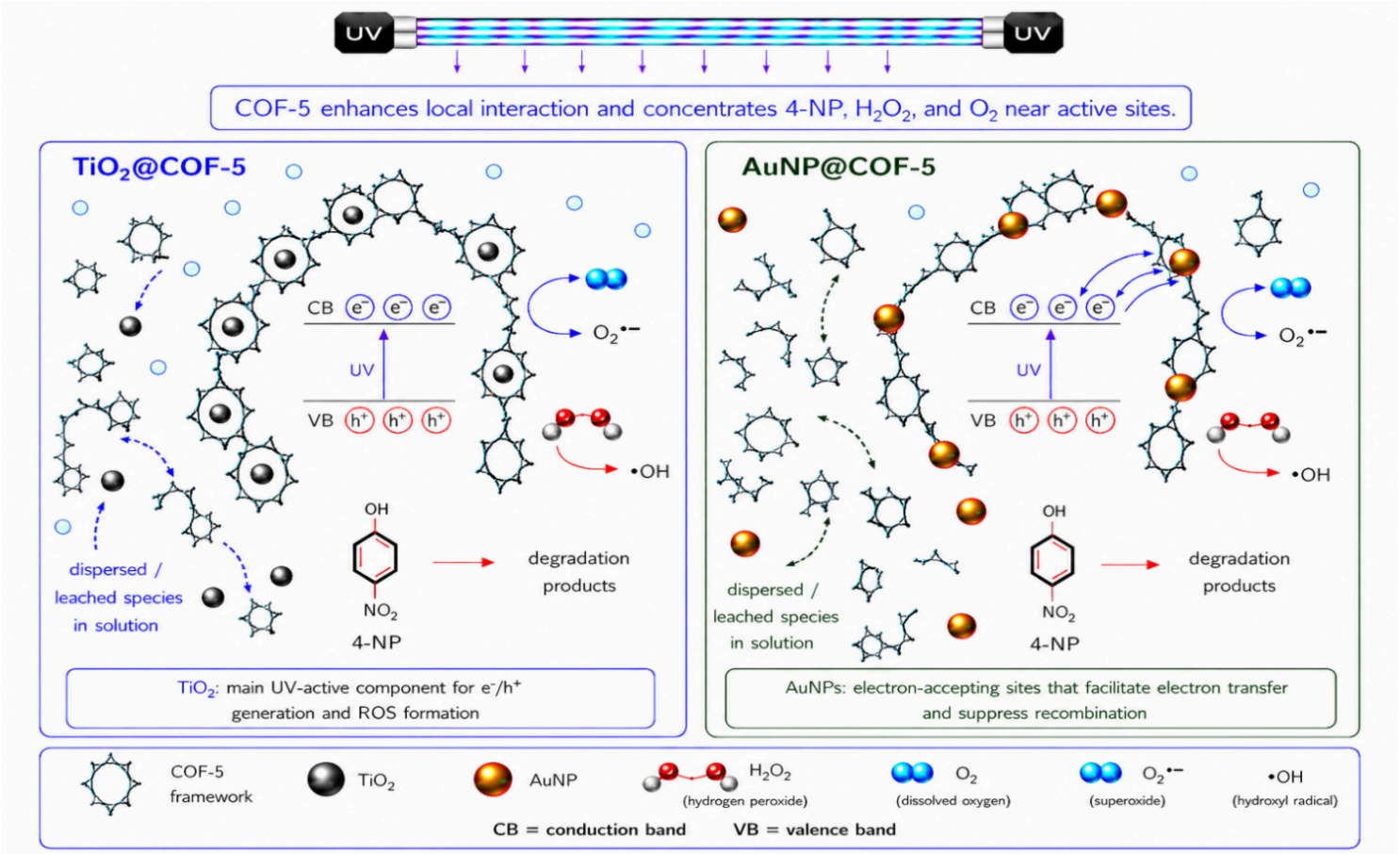

Figure 5

Photodegradation mechanism on the photocatalyst

Supplementary Files

This is a list of supplementary files associated with this preprint. Click to download.

- Supplementary.docx